RSC Advances

PAPER

View Article Online
View Journal | View Issue

Cite this: *RSC Adv.*, 2026, **16**, 18974

A new insight of a pH-dependent fluorescence switching mechanism and the novel radical scavenging ability of nitrogen-doped citric acid-based carbon dots

Bao Bui-Thi,[a] Mai Anh Ngo,[a] Dao Dang Thi Bich,[a] Van-Thao Ta,[b] Hoa Tran-Khanh,[c] Thi Bich Viet Nguyen,[a] Nga Tran-The[a] and Ngan Nguyen-Bich *[a]

In this report, nitrogen-doped citric acid-based carbon dots (N-CAdots) were synthesized, and their apparent pK_a values as well as a fluorescence switching pK_a were systematically determined, providing new insight into the pH-dependent fluorescence switching mechanism of these materials. In addition, the N-CAdots presented as an efficient radical scavenger in mildly alkaline medium, exhibiting high reactivity toward the peroxymonocarbonate radical ($CO_3^{\bullet-}$) compared with *N*,*N*-dimethylaniline. This property enables their application as a fluorescence sensor for hydrogen peroxide (H_2O_2). Based on a simple reaction system involving N-CAdots, H_2O_2, HCO_3^-, and Co^{2+}, the sensor demonstrates high sensitivity toward H_2O_2 at low, biologically relevant concentration levels in serum matrices. Furthermore, a novel modified glucose oxidase method was successfully developed by coupling enzymatic H_2O_2 generation with N-CAdots as the fluorescence probe, enabling glucose determination in serum. This versatile sensing platform offers a promising alternative strategy for the detection of H_2O_2 and H_2O_2-generating analytes by exploiting the radical scavenging properties of N-CAdots. These sensors highlight sustainable analytical approaches that support global efforts to reduce the carbon footprint of chemical measurements.

Received 14th January 2026
Accepted 23rd March 2026

DOI: 10.1039/d6ra00349d

rsc.li/rsc-advances

Introduction

Carbon dots (CDs) and their extraordinary photoluminescence properties make them promising candidates for fluorescence-based analytical methods.[1] The vast majority of material properties of CDs have been well documented, encompassing FT-IR, EDX, and X-ray spectra.[2–4] Despite its significance, the pK_a, a crucial parameter, has rarely been reported. For example, Zhang *et al.* reported a pK_a value of CDs with simple surface groups based on the potentiometric titration data analyzed using the Henderson–Hasselbalch equation.[5] In fact, CDs usually possess abundant surface functional groups, especially when doped with nitrogen (N-CDs) or other heteroatoms. On the other hand, in addition to the carbon core, the surface groups play a crucial role in the fluorescence (FL) properties of CDs,[6,7] which are dependent on pK_a values. Therefore, pK_a value determination is important, as it not only elucidates fundamental material properties but also provides valuable mechanistic insights into the fluorescence (FL) properties of CDs.

Hydrogen peroxide (H_2O_2) is one of the most important molecules capable of producing reactive oxidant species in biological systems.[8] H_2O_2 plays a major role in redox signalling that controls many cellular pathways determining cell fate, including cellular metabolism, proliferation, stress responses, cell survival (oxidative eustress), and inflammation, growth arrest, cell death, tumour growth, and metastasis (oxidative distress).[9,10] The conversion between oxidative eustress and distress depends on the H_2O_2 concentration. For instance, the extracellular H_2O_2 concentrations below approximately 100 μM and above 10 μM correspond to oxidative eustress and distress, respectively.[9–12] Numerous diseases are associated with excessive H_2O_2 release into the bloodstream. Consequently, the detection of H_2O_2 in serum is potentially valuable as a biomarker for a range of diseases, including thyroid disorders, Alzheimer's disease, asthma, chronic obstructive pulmonary disease, and cancer.[13–15] Methods for H_2O_2 detection are diverse and include titration, colorimetry, fluorescence, chemiluminescence, electrochemistry, chromatography, and NMR spectroscopy.[8,14,16] However, the primary drawbacks of these approaches are limited sensitivity and selectivity within the

[a]*Faculty of Chemistry, Hanoi National University of Education, 136 Xuan Thuy, Hanoi, Vietnam. E-mail: ngannb@hnue.edu.vn*
[b]*Faculty of Medical Technology, Hanoi Medical University, 01 Ton That Tung, Hanoi, Vietnam*
[c]*Faculty of Chemistry and Environment, Thuyloi University, 175 Tay Son, Hanoi, Vietnam*

biological concentration range, as well as complex instrumentation requirements.[8] Therefore, sensors have been developed to detect H_2O_2 at micromolar levels. These sensor devices are typically based on carbonaceous or polymeric substrates, which incorporate composites with heavy metal or metal oxide nanostructures.[17,18] In addition, enzyme-based sensors employing horseradish peroxidase, cytochrome C, and catalase have been reported.[8,12] The main disadvantages of these sensors arise from fabrication processes involving heavy metals or metal oxides. Moreover, the enzyme activity is susceptible to pH, temperature, buffer conditions, and long-term stability.[12] Therefore, developing a simple method to detect H_2O_2 at low concentrations, particularly within the biological range, remains an important research challenge.

CDs are promising materials that have been primarily studied for H_2O_2 detection based on their electrochemical properties.[19,20] In contrast, the application of CDs as FL sensors for H_2O_2 analysis remains limited. Existing methods are often complex, requiring post-synthesis surface modification or operation under harsh conditions, such as pH 1–3 in the Fenton reaction.[21–23] These studies propose that CD fluorescence quenching is caused by hydroxyl ($HO^{\bullet}$), one of the major reactive oxygen species (ROS) generated *via* the Fenton reaction. These studies reveal that CDs can act as radical scavengers. In this context, H_2O_2 is considered a primary ROS precursor. However, to date, no studies have reported fluorescence quenching of CDs by H_2O_2-derived ROS under mild alkaline pH conditions, which are more suitable for analytical applications and biological matrices.

In contrast to the Fenton reaction, which is inefficient in forming radicals in basic medium, the H_2O_2–HCO_3^- reaction system catalyzed by Co^{2+} has recently been reported to efficiently produce ROS under mildly alkaline conditions. The proposed reaction are as follows:

$$H_2O_2 + HCO_3^- \rightleftharpoons HCO_4^- + H_2O \quad (1)$$

$$HCO_4^- + Co^{2+} \rightarrow CO_3^{\bullet -} + HO^- + Co^{3+} \quad (2)$$

$$HCO_4^- + Co^{2+} \rightarrow HO^{\bullet} + CO_3^{2-} + Co^{3+} \quad (3)$$

In this system, H_2O_2 transfers the peroxide moiety (–O–O–) to HCO_3^- to form peroxymonocarbonate (PMC, HCO_4^-).[24–29] Therefore, HCO_4^- act as a secondary ROS precursor. Notably, PMC is formed *in situ* in H_2O_2 solution with the presence of HCO_3^-. The production of carbonate radical anions ($CO_3^{\bullet -}$) and hydroxyl radicals ($HO^{\bullet}$) occurs simultaneously. Under specific conditions, the concentration of $CO_3^{\bullet -}$ has been reported to be approximately 1000 times higher than that of $HO^{\bullet}$.[30] Furthermore, the lifetime of $CO_3^{\bullet -}$ is longer than that of $HO^{\bullet}$,[31] suggesting that CDs fluorescence could be quenched in this system. Nevertheless, this phenomenon has not yet been reported.

In this study, we synthesized nitrogen-doped citric acid-based carbon dots (N-CAdots) based on our previous report.[29] We subsequently focused on: (i) determining the apparent pK_a of N-CAdots; (ii) investigating fluorescence quenching of N-CAdots fluorescence in the presence of ROS *via* their radical scavenging activity towards H_2O_2-derived ROS under mild alkaline conditions; (iii) developing new methods for H_2O_2 and glucose determination in serum matrices.

Experimental

Materials

All reagents were of analytical grade. Citric acid anhydrous (CA, $C_6H_8O_7$), ammonium hydrogen carbonate (AHC, NH_4HCO_3), sodium acetate (CH_3COONa), acetic acid (CH_3COOH), sodium chloride (NaCl), potassium chloride (KCl), disodium hydrogen phosphate (Na_2HPO_4), potassium dihydrogen phosphate (KH_2PO_4), sodium hydroxide (NaOH), hydrogen chloride (HCl), sodium azide (NaN_3), hydrogen peroxide (H_2O_2), borax ($Na_2B_4O_7 \cdot 10H_2O$), oxalic acid ($C_2H_2O_4$), *N*,*N*-dimethylaniline (DMA) were purchased from Merck. Bovine serum albumin (BSA) and glucose oxidase (GOx) were purchased from Biobasic. Metal standard solutions (1000 ppm) including Co^{2+}, Zn^{2+}, Cr^{3+}, Ni^{2+}, Mn^{2+}, Cu^{2+}, and Fe^{3+} in 0.5 M HNO_3 were obtained from Merck.

Fluorescence spectra were recorded using an FL8500 Molecular Fluorescence Spectrophotometer (PerkinElmer). Fluorescence emission intensity was collected at 438 nm with an excitation wavelength of 345 nm using quartz cuvettes (1.0 cm path length). Other instrumental parameters were kept constant: photomultiplier tube voltage of 400 V and the slit width of 5 nm. pH values were measured using a pH/ISE benchtop meter (inoLab pH/ION 7320, Xylem Analytics). Ammonium concentrations were measured using an ammonium-selective electrode (WTW, Xylem Analytics).

N-CAdots preparation

Based on our previous work,[29] N-CAdots were synthesized from CA and NH_4Cl, with NH_4Cl replaced to NH_4HCO_3 as a nitrogen-doped source. Reactions were performed in a microwave synthesis reactor (Monowave 200, Anton Paar, 800 W). The reaction between CA and NH_4^+ was systematically investigated by varying the following parameters: (i) the CA: NH_4^+ molar ratio (5.0 mM CA with NH_4^+ concentration of 0, 20, 40, 60, 80 mM, pH 8) at 200 °C for 5 min; (ii) reaction pH (2, 4, 5, 6, 8, 10, 11, and 12) at 5.0 mM CA and 80 mM NH_4^+, 200 °C for 5 min; (iii) reaction time (5.0 mM CA, 40 mM NH_4^+, pH 8) at 200 °C for 2, 4, 6, 8, 10, 15, and 20 minutes. The resulting dots were purified using regenerated cellulose dialysis membranes (Merck, molecular weight cut-off 3.5 kDa) for 3 hours.

pK_a values determination

The pK_a values were determined by analysing potentiometric and fluorescent titration data. pH measurements were recorded at 25.0 ± 0.5 °C. The titration data were analyzed using Curtipot software[32] to calculate the apparent pK_a values of N-CAdots. The software optimized the target values to fit the experimental data using the regression analysis while accounting for ionic strength. NaOH and HCl titrant solutions were standardized by potentiometric titration with oxalic acid and borax, respectively. A 5.0 mL aliquot of studied solutions were titrated potentiometrically or fluorometrically with NaOH and HCl.

Radical scavenging activity of N-CAdots

The radical scavenging activity of N-CAdots was evaluated by fluorescence quenching in reaction systems containing N-CAdots and H_2O_2. The quenching effect was quantified using the ratio of the fluorescence intensity of the blank solution (I_0) to that of the sample (I), expressed as I_0/I. Three experiments batches were conducted: (i) the effect of reaction media, including PBS 1× (8 g per L NaCl, 0.2 g per L KCl, 1.44 g per L Na_2HPO_4, 0.245 g per L KH_2PO_4), acetate (100 mM CH_3COONa), and AHC (100 mM NH_4HCO_3) at various pH values (adjusted using NaOH or HCl) with and without Co^{2+}; (ii) the effect of transition metal ion catalysts (Co^{2+}, Zn^{2+}, Cr^{3+}, Ni^{2+}, Mn^{2+}, Cu^{2+}, and Fe^{3+}, all at 1.85 ppm) in 100 mM AHC at pH 7.8; (iii) the effect of reaction time in 100 mM AHC buffer at pH 7.8 and 8.2, compared with DMA at 5 and 25 °C. The reaction setup included N-CAdots, H_2O_2, and, when applicable, the reaction medium, serum, and transition metal ions.

H_2O_2 and glucose detection

Stock solutions of H_2O_2 and at various glucose concentrations were prepared in a simulated serum matrix and used throughout the experiments. A stock of simulated serum matrix consisted of PBS 1× (pH 7.4), 4% BSA, and 0.05% NaN_3. Reaction mixture for H_2O_2 or glucose detection included AHC buffer pH 7.8 or 8.2, N-CAdots, Co^{2+}, and either H_2O_2 or glucose–glucose oxidase. The mixture was incubated, and fluorescence measurements were performed after 1 min for H_2O_2 and 20 min for glucose. The blank solution contained AHC, N-CAdots, Co^{2+}, and serum matrix. Optimization of the detection conditions for both H_2O_2 and glucose was systematically investigated. For H_2O_2 detection, the effect of reaction time, H_2O_2 concentration (0.06–60 mM), and serum fraction (0.94–18.87%) were studied. The Co^{2+} concentrations were optimized (*e.g.*, 0–4.7 ppm Co^{2+}). For glucose detection, optimization included components, GOx concentration (*e.g.* 0.95 and 1.9 μg mL^{-1} enzyme), and reaction kinetics. Calibration curves were constructed based on the H_2O_2 or glucose concentration *versus* I_0/I value under optimized conditions. Following the AOAC guidelines, the limit of detection (LOD) and limit of quantification (LOQ) were calculated using the standard deviation of 10 blank measurements.[33] Repeatability and recovery were evaluated at 3 concentration levels, with each level replicated seven times. Performance criteria for repeatability and recovery were assessed according to concentration (mass fraction), as specified by AOAC guidelines.[33]

Result and discussion

Synthesis optimization and N-CAdots properties

As demonstrated in our previous study, nitrogen doping using an AHC endowed N-CAdots with good fluorescence characteristics, including high quantum yield, strong emission fluorescence intensity, and long-term stability.[29] In that system, bicarbonate played as a buffer agent, maintaining a mildly basic reaction environment without significantly altering the concentration (data not showed). Building on these finding, the present work aims to investigate the synthesis of N-CAdots from citric acid (CA) using a simpler nitrogen source, namely ammonium ion (NH_4^+), which can inherently provide buffering capacity under mildly basic conditions.

In the absence of bicarbonate, the optimized synthesis conditions for CA–NH_4^+ system exhibited trends similar to those observed for CA–AHC system. The details are as follows: the optimal CA : NH_4^+ mole ratio from 1 : 8 to 1 : 10, with reaction time of 15 minutes at pH ≈ 8 and a temperature of 180–220 °C (Fig. 1). These results clearly demonstrate the crucial role of nitrogen doping in the formation of N-CAdots, as no detectable fluorescence was observed in the absence of nitrogen source (ratio 1 : 0 in Fig. 1A). The synthesis effectiveness reached a maximum within the pH range of 8–10, consistent with the favorable condition for cyclic structure formation reported previously.[29] In contrast, acidic condition significantly suppressed the synthesis, particularly at pH values below 5 (Fig. 1B). The previous work showed that the fluorescence of N-CAdots can be quenched under acidic conditions (pH ≈ 4 and lower), therefore, the reaction mixtures were initially prepared at pH 2 and 4 then the post-synthesis solutions were subsequently adjusted to pH values above 5 to restore fluorescence. Nevertheless, no fluorescence was detected confirming that N-CAdots were not formed under these acidic synthesis conditions. The carbon footprint under the optimal synthesis

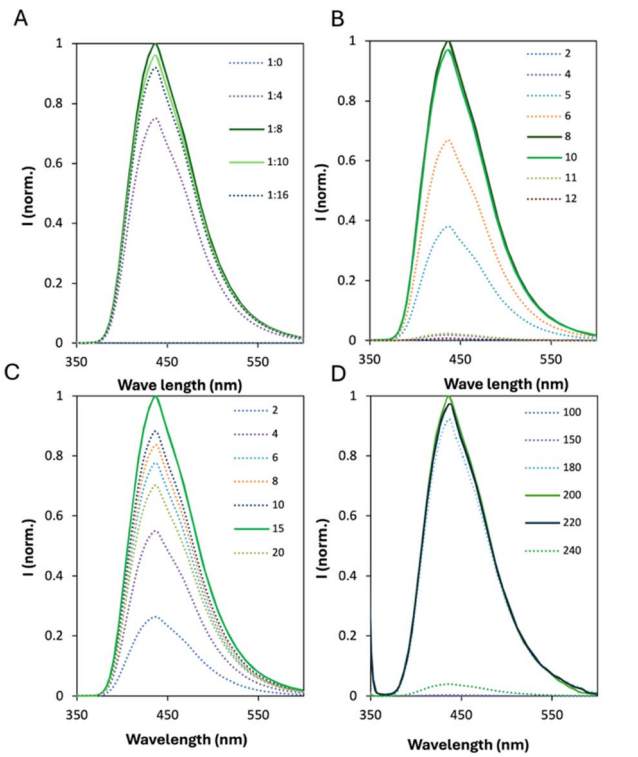

Fig. 1 The fluorescence spectra of N-CAdots solutions under different synthesis conditions. (A) The effect of CA : NH_4^+ ratios (1 : 0, 1 : 4, 1 : 8, 1 : 12, 1 : 16). (B) Different pH conditions (2, 4, 5, 6, 8, 10, 12). (C) Varying synthesis time (2, 4, 6, 8, 10, 15, 20 min). (D) Influence of temperature (100, 150, 180, 200, 220, 240 °C). The optimal conditions are presented the solid lines, the other are in dot lines.

condition, raising mainly form the electrical energy consumption (15 min of 800 W microwave-assisted synthesis), was calculated according to method reported in ref. 29 to be 4.73 g CO_2 per mL of N-CAdots solution. The material properties for N-CAdots in this work including FT-IR spectrum, TEM, UV-vis spectrum, emission independent excitation spectra (SI Fig. S1) were also similarly to those in N-CAdots synthesized form CA and AHC.[29]

Several studies have reported the synthesis of CDs from CA and ammonia; however, these works did not comprehensively optimize the synthesis parameters, despite their crucial influence on the fluorescence properties of CDs.[34–36] Notably, although microwave-assisted synthesis was employed in both cases, Wang *et al.* reported CDs exhibited excitation-dependent fluorescence emission and selective sensing of Fe^{3+} ion,[34] whereas the N-CAdots developed in our work displayed excitation-independent emission and strong selectivity toward Hg^{2+}.[29] Similarly, Zhang *et al.* synthesized CDs *via* a hydrothermal route that also resulted in excitation-dependent fluorescence behaviour, while retaining the selectivity toward Hg^{2+}.[35] In contrast, Reckmeier *et al.* reported that CDs prepared from CA and aqueous or supercritical ammonia under hydrothermal synthesis conditions consisted of amorphous aggregates of molecular fluorophores with an average particle size of approximately 18 nm;[36] whereas our N-CAdots and those reported in other studies typically exhibit average diameters below 5 nm. These pronounced variation in optical properties, particle size, and sensing selectivity, despite the use of similar precursors or synthesis techniques, underscore the strong dependence of carbon dot characteristics on precise synthesis conditions and methodologies.

Apparent pK_a determination

The pK_a values of CDs surface groups are a crucial parameter of this material, but it is not commonly studied, and thus, the data on the pK_a values of CDs are currently unavailable. The pK_a plays an important role in the prediction of an effective fluorescence medium for CDs. However, CDs are known to be carbon-core materials which have various surface functional groups. The determination of an individual pK_a value for each group seems impossible and holds little scientific significance. Therefore, we focus our attention on determining some apparent pK_a values of N-CAdots for groups with distinctly different pK_a such as carboxylic acid, phenol, ammonium salt of amine (*e.g.*, $-NH_3^+$), or amide.

In this work, acid–base titration data of the studied systems were analysed using a regression-based approach to determine simultaneously a pK_a value and concentration of each functional group. The method was first validated by fitting titration curves to determine both the concentrations and pK_a values of purified CA and NH_4^+ in three systems, examined without and with 3 hours of dialysis: (i) 5 mM CA solution; (ii) 50 mM NH_4^+ solution, and (iii) a mixed solution containing 5 mM CA and 50 mM NH_4^+. The results showed that the determined pK_a values of CA in individual solution and in the CA/NH_4^+ mixture, both without and with dialysis, were not statistically different ($p = 0.085$ for pK_{a1}, $p = 0.110$ for pK_{a2}, and $p = 0.146$ for pK_{a3}; all >0.05). Accordingly, all datasets were pooled to determine the apparent pK_a values of CA, yielding p$K_{a1} = 3.54 \pm 0.20$, p$K_{a2} = 5.00 \pm 0.12$, and p$K_{a3} = 6.52 \pm 0.10$. Similarly, the pK_a of NH_4^+ showed no significant difference between pre- and post-dialysis ($p = 0.22$), and a pK_a value of 9.33 ± 0.05. These values were also reproduced in the mixed CA/NH_4^+ systems under both conditions (SI Table S1). Overall, the determined pK_a values exhibit good reproducibility and are in close agreement with literature data.[37] In addition, the quantitative results revealed that after 3 hours of dialysis, the concentration of –COOH group in CA solution (three times of CA concentration) decreased from 15.0 ± 0.4 mM to 9.3 ± 0.4 mM, corresponding to a reduction of approximately 38%. While concentrations of NH_4^+ decreased from 51.7 ± 2.1 mM to 10.2 ± 0.5 mM, corresponding to an about 80% reduction (SI Table S1). The calculated pre-dialysis concentrations of both –COOH group of CA and NH_4^+ in closely matched the values prepared from purified reagents. For NH_4^+, the concentration was further confirmed using an NH_4^+-selective membrane electrode. These results validate the regression-based titration method for simultaneous determination of CA (or –COOH group) and NH_4^+ concentrations, as well as their corresponding pK_a values. On this basis, the validated approach was subsequently applied to determine the apparent pK_a values of synthesized N-CAdots.

Secondly, the potentiometric titration curves of the synthesized N-CAdots solution before dialysis were analyzed. In this solution, the concentration of –COOH group was determined to be (11.9 ± 0.5) mM, corresponding to about 20.1% decrease relative to the value before synthesis. The reduction can be attributed to the partial conversion of carboxyl groups into polymeric carbon structures or incorporation into the carbon-core of N-CAdots. For the solution after dialysis, the –COOH concentration decreased only slightly (by approximately 8.3%) compared to the pre-dialysis solution. Comparing between pre- and post-dialysis, the decrease level of –COOH concentration in N-CAdots was much less than that in the CA itself solution. This indicates that the majority of the detected –COOH groups are associated with the surface of N-CAdots. Once bound to the carbon-core, these –COOH groups become part of larger molecular structures and are therefore unable to pass through a dialysis membrane.

Potentiometric analysis of the dialysed N-CAdots solution yielded pK_a values of residual CA (3.34 ± 0.36), (5.10 ± 0.12), (6.37 ± 0.17), as well as additional pK_a values at (2.24 ± 0.19), (4.41 ± 0.22), (5.75 ± 0.16), and (7.04 ± 0.19). These additional dissociation constants suggest the appearance of –COOH groups on the surface of the carbon core in modified electronic environment, resulting in acidic strengths distinct from those of the original –COOH groups of CA, or possibly arising from other surface acidic functionalities. Notably, these values are closely spaced, such that they cannot be individually resolved using the Henderson–Hasselbalch equation. This observation is consistent with the report by Zhang *et al.*, who obtained a single apparent pK_a value of 4.50 for CQDs.[5]

A detailed analysis of the synthesized solution further revealed that the concentration of NH_4^+ remained nearly

unchanged within the detection limit of the potentiometric titration method. This observation indicates that the overall extent of nitrogen incorporation into the N-CAdots is relatively low, despite its pronounced influence on the fluorescence properties of N-CAdots. Following dialysis of the N-CAdots solution, the decrease in NH_4^+ concentration was comparable to that observed for dialysed pure NH_4^+ solution, with the measured concentration of 10.0 ± 0.9 mM and a pK_a of 9.34 ± 0.03. Notably, potentiometric analysis of the dialysed N-CAdots solution revealed an additional pK_a value at 9.69 ± 0.12, which is close to that of NH_4^+. This value is therefore attributed to pronated nitrogen-containing surface functionalities, such as ammonium salts of amine groups, present on the surface of the N-CAdots (SI Table S2 and Fig. S2).

Interestingly, the analysis of the pH-dependent FL titration of N-CDs enabled the estimation of a critical apparent pK_a value that governs the fluorescence switching behaviour of the N-CAdots' FL. Utilizing the second-derivative method, the apparent pK_a value for the switching equilibrium: N-CDs-H^+ (off-state) ⇌ N-CDs (on-state) + H^+ (p$K_{a\text{-sw}}$), was determined. Across results from analysing FL titration data for solutions with two distinct N-CAdots concentrations, an average apparent p$K_{a\text{-sw}}$, value of 4.45 ± 0.03 was obtained (SI Fig. S3). This result is remarkably close to one of the newly identified pK_a values derived from potentiometric titration. The FL titration curves and corresponding p$K_{a\text{-sw}}$ indicate that surface functional groups with pK_a values within the basic range do not govern the pH-based fluorescence switching. Instead, these basic functionalities significantly contribute to enhancing the FL intensity of N-CAdots through nitrogen doping. Conversely, the pronounced pH-dependent fluorescence behavior observed in the acidic region suggests that the protonation–deprotonation processes of hydroxyl-containing surface groups play a dominant role. Protonation of –OH groups can directly perturb the conjugated aromatic system, thereby modulating the electronic structure and fluorescence response. This interpretation is supported by analogous small-molecule systems, such as 4-methyl-8-hydroxyquinoline (pK_a = 4.67), 3-hydroxyquinoline (pK_a = 4.30), and 3-hydroxypyridine (pK_a = 4.80),[37] in which protonation or deprotonation of the –OH groups alters the electron density of the nitrogen-containing heterocyclic aromatic framework. The pK_a values of these compounds are comparable to p$K_{a\text{-sw}}$ determined for the N-CAdots. These findings are also consistent with the pH-dependent UV-vis absorption behavior reported in our previous study. At low pH (pH = 2.3), the absorbance peak at 234 nm, assigned to the π–π* transition of the aromatic C=C group, disappears due to the protonation of surface groups.[29] Collectively, the apparent p$K_{a\text{-sw}}$ emerges as a key parameter governing the fluorescence switching mechanism of N-CAdots synthesized using this approach.

The radical scavenger ability of N-CAdots

As discussed in the introduction, the fluorescence quenching of carbon quantum dots by H_2O_2 under acidic conditions has been widely attributed to the generation of ROS. In the present study, we focus on the behavior of N-CAdots in the presence of ROS under mildly basic conditions. As showed in Fig. 2, the FL of N-CAdots remains essentially unchanged in the presence of H_2O_2 alone in all investigated media ($I_0/I \approx 1$), indicating that H_2O_2 neither directly generates ROS nor reacts with N-CAdots under these conditions. Consequently, to demonstrate the interaction between N-CAdots and ROS, H_2O_2 must be activated *via* two approaches. First, H_2O_2 can be catalytically activated by transition metal ions (TMIs), where it functions as a primary ROS precursor through direct catalytic processes (primary reactions). Second, H_2O_2 can participate in secondary reactions with suitable substrates to form peroxo (–O–O–) intermediates, which act as secondary ROS precursors and subsequently decompose to generate ROS.

The formation of ROS *via* primary reaction was examined in the N-CAdots–H_2O_2–Co^{2+} system in DI water, where slight fluorescence quenching was observed (I_0/I = 1.30 ± 0.05). This result suggests that Co^{2+} catalytically activates H_2O_2 to produce ROS, including hydroperoxyl ($^{\bullet}OOH$), superoxide ($O_2^{\bullet-}$), and other moderate-to-strong oxidizing agents, such as Co(III). The catalytic process was proposed to proceed *via* the formation of a cobalt–peroxo intermediate, $[(H_2O)_4Co(II)(OOH)(H_2O_2)]$.[25] These reactive species can be responsible for the observed fluorescence quenching of the N-CAdots. When PBS was used in place of DI water, the I_0/I ratio decreased to 1.06 ± 0.02. Raineri *et al.* reported that, the PBS buffer can inhibit the peroxidase-like activity.[38] These results demonstrated that the FL quenching of N-CAdots *via* primary reaction at neutral pH is weak and that the FL signal can be preserved in the presence of PBS.

Secondary reactions were investigated under mildly alkaline conditions using AHC (pH 8.2) and acetate (pH 8.3). In acetate medium, only weak fluorescence quenching was observed (I_0/I

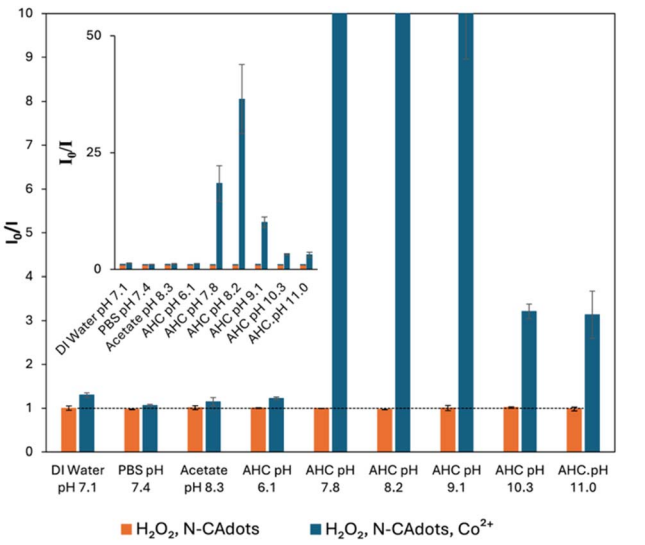

Fig. 2 Magnified view of the N-CAdots scavenging activity under various reaction conditions. The inset presents the full image. The different buffers utilized were phosphate-buffered saline (PBS, pH 7.4), acetate (pH 8.3), and ammonium hydrogen carbonate (AHC) (pH 6.1, 7.8, 8.2, 9.1, 10.3, and 11.0). The base line corresponding to 1 or the value of N-CAdots FL in DI water.

$= 1.14 \pm 0.10$). This limited quenching effect can be explained by the fact that the formation of peroxyacetic acid (PAA), as described by the equation $CH_3COOH + H_2O_2 \rightleftharpoons CH_3COOOH + H_2O$, is favored in acidic rather than alkaline conditions.[39] The –O–O– bond in PAA is prone to homolytic cleavage, generating acetoxyl ($CH_3C(O)O^{\bullet}$) and ($HO^{\bullet}$) radicals, a process widely exploited in advanced oxidation processes for organic pollutant removal under acidic conditions.[40] Conversely, in the AHC medium, a pronounced FL quenching was observed, with the I_0/I ratio reaching approximately 36.5. In the H_2O_2–HCO_3^-–Co^{2+} reaction system, PMC is formed and subsequently decomposed into highly reactive radical species, predominantly $CO_3^{\bullet-}$ and $HO^{\bullet}$, according to eqn (1)–(3).[41] These results demonstrate the strong sensitivity of N-CAdots toward ROS generated under mildly alkaline conditions through the PMC pathway.

The reaction in AHC medium was further investigated at various pH values. At pH 6.1, the reaction exhibited only a weak response, with an I_0/I ratio comparable to those observed in PBS and acetate media. A pronounced increase in FL quenching was observed at pH 7.8, reaching a maximum at pH 8.2. Beyond this point, the I_0/I ratio decreases sharply at pH 9.1 and continues to decline at pH 10.3, eventually stabilizing at approximately 3.0 at pH 11.0. Despite this decrease, the I_0/I value remained significantly higher than unity, indicating sustained ROS activity. This pH-dependent trend of N-CAdots FL quenching is consistent with the reported pH dependence of PMC formation, which is governed by the availability its precursor, bicarbonate.[24] The observed decrease in the I_0/I at higher pH values is likely associated with a reduction in the concentration of soluble $[Co(H_2O)_6]^{2+}$ ions. This decrease can be attributed to the precipitation of cobalt species, such as $Co_2(CO_3)(OH)_2$ and $Co(OH)_2$ at pH values between 9 and 11.[42] These observations reflect the pH-dependent behavior of ROS generation in the H_2O_2–HCO_3^-–Co^{2+} reaction system and further demonstrate the capability of N-CAdots to sensitively probe variations in ROS levels, as well as their effective radical scavenging properties.

To further investigate the effect of TMIs in catalyzing ROS formation *via* the PMC pathway, a series of metal ions were evaluated under identical reaction conditions (H_2O_2, HCO_3^-/AHC, pH 7.8, and the respective TMIs). The results showed that Co^{2+} yielded an I_0/I value approximately nine times higher than those obtained with other metal ions, including Zn^{2+}, Cr^{3+}, Ni^{2+}, Mn^{2+}, Cu^{2+}, and Fe^{3+} (SI Fig. S4). Although these TMIs are capable of catalyzing the conversion of PMC into radical species in the H_2O_2–HCO_3^- system, their catalytic efficiencies strongly depend on the reaction conditions. For instance, Co^{2+} exhibits the highest catalytic activity in the neutral to mildly alkaline pH range, where the reaction is rapid and exothermic, whereas Fe^{3+} is most effective under acidic conditions (pH 2–3) and Cu^{2+} at strongly alkaline pH values (pH $\approx$ 10).[43,44] These results clearly demonstrate that ROS formation *via* the PMC pathway is significantly enhanced by Co^{2+} under the present experimental conditions, in agreement with previous reports highlighting the pivotal role of Co^{2+} in ROS generation from PMC.[26,45–47]

From these observations, together with evidence that ROS generation *via* the PMC pathway results in $CO_3^{\bullet-}$ concentration exceeding that of $HO^{\bullet}$ by up to three orders of magnitude (approximately 1000-fold),[30] N-CAdots are proposed to be particularly sensitive toward carbonate radicals. The radical scavenger ability of N-CAdots was further evaluated by comparison with *N*,*N*-dimethylalanine (DMA) a well-known radical scavenger with a high reaction rate constant toward carbonate radicals (1.8×10^9 M^{-1} s^{-1}).[48,49] Under optimal PMC-mediated radical generation conditions, both N-CAdots and DMA exhibited rapid radical scavenging. As showed in Fig. 3, the I_0/I ratio was indistinguishable between 5 and 25 °C. Notably, however, the I_0/I value for N-CAdots was approximately four times higher than that observed for DMA, demonstrating the superior radical-scavenging efficiency of N-CAdots under these conditions.

In summary, the N-CAdots–HCO_3^-–Co^{2+} system represents a promising platform for H_2O_2 detection under mildly alkaline conditions. In this system, the N-CAdots act as efficient radical scavengers, enabling the direct detection of H_2O_2 through Co^{2+}-catalyzed PMC pathway.

H_2O_2 detection

Effect of reaction time. The effect of reaction time on the N-CAdots–HCO_3^-–Co^{2+}–H_2O_2 system was evaluated at pH 7.8 and pH 8.2. In both cases, the FL quenching occurred immediately (SI Fig. S5) indicating the rapid reaction kinetics. This fast response is comparable to the study by Bakhmutova-Albert *et al.*,[24] who reported that PMC was detectable within the first 400 s and that equilibrium was achieved within approximately 10 min in the presence of a zinc complex.[24] Furthermore, at the same H_2O_2 concentration, the I_0/I value at pH 8.2 was higher than the one at pH 7.8, corresponding to the effect of the AHC buffer pH on PMC formation and subsequent ROS generation.

Matrix effect. To evaluate matrix effect, H_2O_2 was spiked into a serum matrix. Serum albumin, the dominant protein in

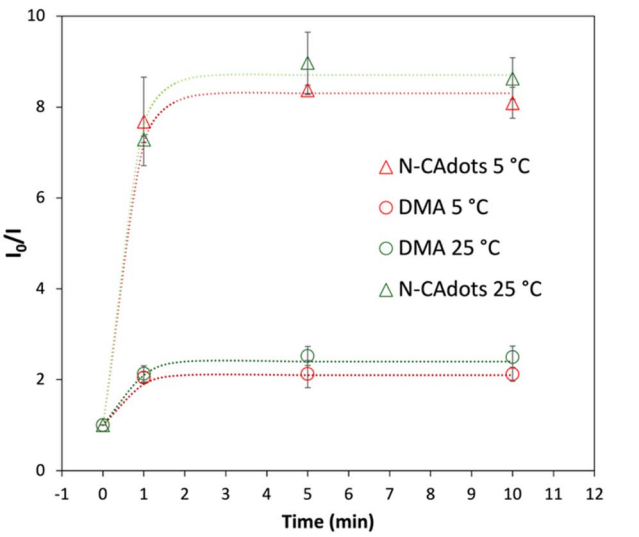

Fig. 3 The comparison of radical scavenging by N-CAdots and DMA. The N-CAdots and DMA concentrations were adjusted to obtain the same initial fluorescence intensity (I_0) value. The reaction were performed at 5 and 25 °C.

serum, is known to act as a radical scavenger and may therefore compete with N-CAdots for reactive radicals.[50] As a result, the serum matrix has the potential to interfere with the FL quenching response of N-CAdots. The results showed that increasing the serum fraction from 0.94 to 18.87% significantly reduced the quenching efficiency of N-CAdots. At a fixed H_2O_2 concentration of 0.06 mM, the I_0/I values were higher at low serum content (0.94 and 1.88%) and significantly decreased at higher serum fractions (9.43 and 18.87%). At serum content of 9.43 and 18.87% of serum, there was no discriminable difference in FL intensities, with I_0/I value remaining only slightly above unity (Fig. 4). This trend was also observed at other H_2O_2 concentrations, demonstrating the strong scavenging effect of serum components on the ROS-mediated FL quenching of N-CAdots.

Notably, these results also reveal that the pronounced dependence of FL quenching efficiency on H_2O_2 concentration (0.06–60 mM) at constant serum levels. This effect was particularly evident at low serum fractions (*e.g.* 0.94 and 1.88%), where the radical scavenging activity of N-CAdots surpassed that of the serum proteins. Specifically, at 0.94% serum, the I_0/I value at 0.06 mM was approximately 14 times higher than those observed at higher H_2O_2 concentrations, for which no significant difference in I_0/I was detected (Fig. 4). This phenomenon can be a result of the radical–radical recombination at high radical concentrations, as described by the reaction $A^{\bullet} + HOO^{\bullet} \rightarrow O_2 + AH$.[51] In addition, the excess H_2O_2 can inhibit the radical chain oxidation process.[52] Thus, based on these findings, optimization of the H_2O_2 concentration is essential to for observing the fluorescence quenching measurements. In this study, H_2O_2 concentrations were therefore maintained below 0.06 mM (or 60 μM) for subsequent experiments.

Effect of Co^{2+} concentration. In our previous study, Co^{2+} was shown not to affect the intrinsic fluorescence of N-CAdots at concentrations up to 14 ppm.[29] Therefore, variations in the I_0/I ratio of the N-CAdots–H_2O_2–HCO_3^-–Co^{2+} at different Co^{2+} concentrations observed in Fig. 5 can be attributed solely to the catalytic activity of Co^{2+} in ROS generation. In the absence of Co^{2+}, no fluorescence quenching was observed upon addition of H_2O_2. The I_0/I ratio increased significantly with increasing Co^{2+} concentration up to approximately 2 ppm. Beyond this concentration, further increases in Co^{2+} did not result in a substantial enhancement of FL quenching at either pH 7.8 or pH 8.2 (Fig. 5). Therefore, a Co^{2+} concentration of 2 ppm was selected as optimal for catalytic activation.

Method validation. At both pH 7.8 and pH 8.2, the I_0/I ratio showed a dependence on the H_2O_2 concentration. In the wide concentration range, the response was nonlinear (SI Fig. S6). Within the linear range at pH 8.2, the calibration curve was $I_0/I = (0.4836 \pm 0.0009)C_{H_2O_2} + (0.949 \pm 0.002)$ ($R^2 = 0.998$), with a quantification range of 0.77–4.6 μM, LOD and LOQ of 0.25 and 0.77 μM, respectively. At pH 7.8, the linear calibration curve was $I_0/I = (0.363 \pm 0.009)C_{H_2O_2} + (0.82 \pm 0.03)$ ($R^2 = 0.998$), with a quantification range from 1.2 to 9.2 μM H_2O_2, LOD and LOQ of 0.41 and 1.22 μM, respectively (Fig. 6).

These findings are comparable to those reported for carbon dot-based H_2O_2 sensors, particularly those employing Fenton reactions (Table 1). A key advantage of the present method is its ability to achieve reliable detection limits under mildly alkaline conditions, in contrast to the strongly acidic environment typically required for Fenton-based systems. This feature makes the N-CAdots–HCO_3^-–Co^{2+} system a promising candidate for biological and environmental applications where mild conditions are essential.

The method was validated following the AOAC guideline,[33] using calibration curves constructed at both pH 7.8 and pH 8.2.

Method repeatability and recovery were established by analyzing H_2O_2 at concentrations of 1.2, 3.1, and 9.1 μM at pH 7.8 and 0.77, 1.85, and 4.6 μM at pH 8.2. Each concentration level was replicated seven times. The results showed that all tested levels satisfied the AOAC performance criteria for analytical methods (SI Tables S3 and S4), confirming the accuracy, precision, and reliability of the N-CAdots-based assay.

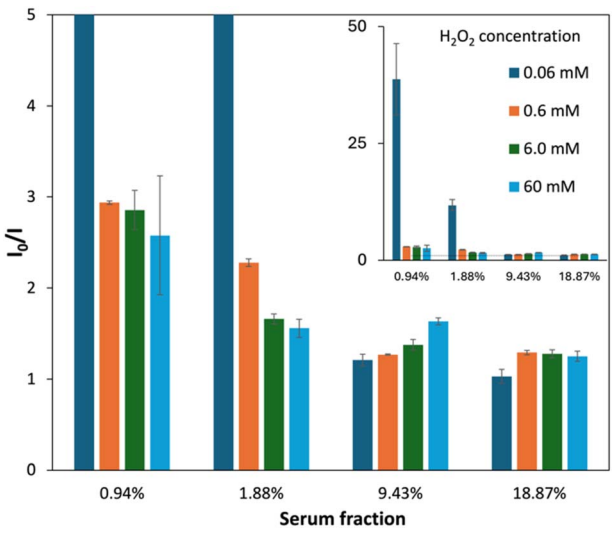

Fig. 4 Magnified view of the effect of serum H_2O_2 concentrations on the radical scavenging activity of N-CAdots. The reaction varied concentrations of H_2O_2 (0.06 to 60 mM) and serum fractions (0.94 to 18.87%). The inset presents the full image.

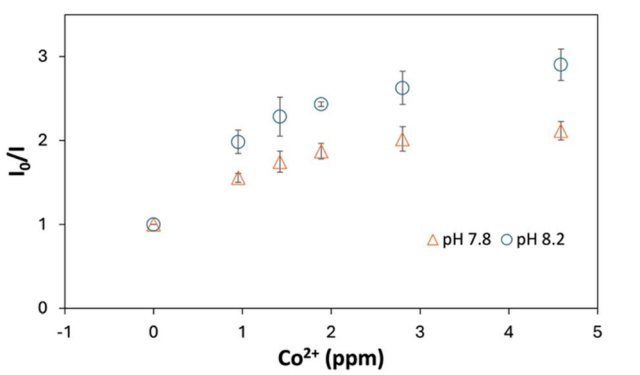

Fig. 5 Effect of Co^{2+} concentration on the I_0/I value at different AHC pH buffer conditions. The I_0/I value was investigated at various condition of Co^{2+} (0 to 4.70 ppm), 100 mM AHC at pH (7.8 and 8.2).

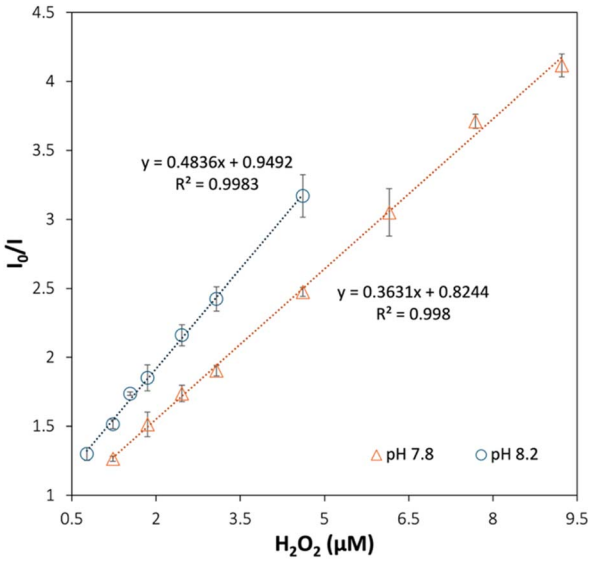

Fig. 6 Calibration curves of H_2O_2 at AHC pH 7.8 and 8.2. The calibration curve was constructed at the optimized condition, which included 100 mM AHC pH 7.8 and 8.2, N-CAdots, 1.85 ppm Co^{2+}.

Glucose sensing by modification GOD method

One of the most widely used methods for glucose determination is the glucose oxidase (GOD) assay, in which GOx catalyzes the oxidation of glucose to gluconate with the concomitant production of H_2O_2. The generated H_2O_2 is subsequently quantified *via* chromogenic reactions involving peroxidase or by electrochemical methods that monitor oxygen consumption or H_2O_2 formation.[53] Consequently, the conventional GOD-based assays typically require an additional enzyme or specialized electrode instrumentation.

Based on the ability of N-CAdots to detect H_2O_2 through radical scavenging properties, we developed a modified GOD-based FL method for glucose determination. In this approach, GOx catalyzes the conversion of glucose into gluconate and H_2O_2, which subsequently participates in the PMC-mediated radical generation pathway, leading to FL quenching of N-CAdots.

Method development. Preliminary screening of reaction components showed that neither glucose nor GOD alone affected the I_0/I ratio. In contrast, when both glucose and GOD were present, the I_0/I value increased dramatically, reaching nearly 90-fold enhancement (Fig. 7). These results indicate that GOx retains enzymatic activity under the optimized reaction conditions for PMC formation and radical generation established in this study. The reaction time was found to depend strongly on the GOx concentration. As shown in Fig. 8A, at a GOx concentration of 1.9 μg mL^{-1}, the I_0/I ratio reached saturation within 10 min, whereas at a lower GOx concentration of 0.95 μg mL^{-1}, saturation required approximately 20 min (Fig. 8A). Therefore, the higher GOx concentration was selected

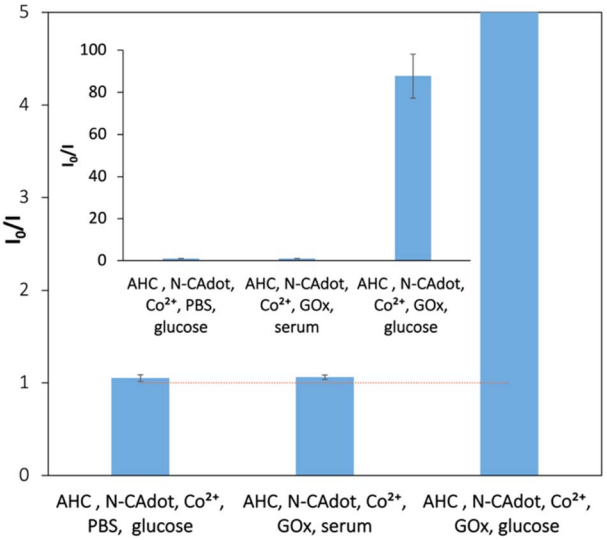

Fig. 7 Magnified view of the evaluation of reaction components in the modified GOD method. The inset presents the full image. The full reaction system included AHC buffer, N-CAdots, Co^{2+}, GOx and glucose, compared to systems lacking GOx or Glucose. The reaction time was 30 minutes.

Table 1 Selected previously reported detection of H_2O_2 by N-Cadots[a]

System	CDs precursors	Post-synthesis modification	pH	Mechanism of detection, analytical method	LOD (μM)	Ref.
Cu-CDs-TMB	Citric acid, urea, Cu^{2+}	Yes	4	Pseudo-peroxidase activity, UV-vis	0.12	54
V_2O_5-CDs-TMB	Candle soot	Yes	3.0	Pseudo-peroxidase activity, UV-vis	0.5	55
CDs-TMB	Phenyl alanine	No	4.2	Pseudo-peroxidase activity, UV-vis	6.5	56
CDs-ODP	L-Histidine	No	4.0	Pseudo-peroxidase activity, PL	0.42	57
P-CDs	Citric acid, ethylenediamine	Yes	4–12	Photo-induced electron transfer, PL	0.084	21
CDs-Fe^{2+}	*N*-Dimethylformamide	No	2–3	Quenching signal by Fenton reaction, PL	3.8	58
GQDs-Fe^{2+}	Polycyclic aromatic hydrocarbon	No	2–3	Quenching signal by Fenton reaction, PL	~1–3	22
CDs-Fe^{2+}	Gelatine	No	2–3	Quenching signal by Fenton reaction, PL	0.1	23
CDs-Fe^{2+}	Gelatine	No	2–3	Quenching signal by Fenton reaction, PL	0.01	59
CDs-AHC-Co^{2+}	**Citric acid, ammonium chloride**	**No**	**8.2**	**Quenching signal via PMC pathway, PL**	**0.25**	This work
			7.8		**0.41**	

[a] TMB: 3,3′,5,5′-tetramethylbenzidine, ODP: octophenyldiamine, P-CDs: proposed sensor, GQDs: graphene quantum dots, UV-vis: ultra-violet absorption spectroscopy; PL: fluorescence spectroscopy.

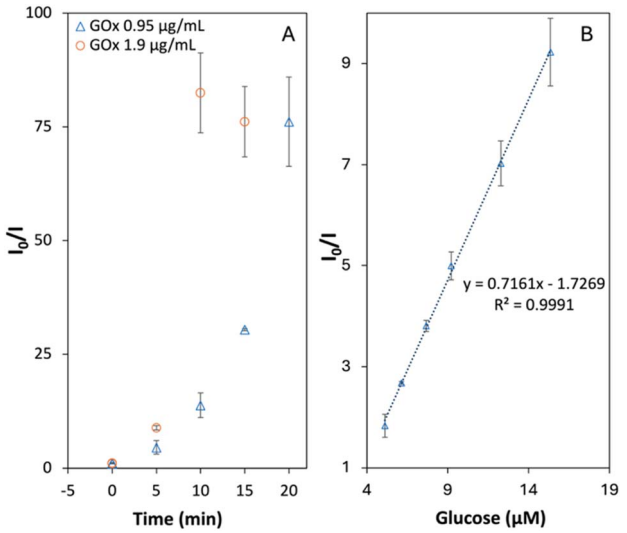

Fig. 8 (A) The effect of GOx concentrations on the modified GOD method. The reaction kinetics were observed at varying concentrations of GOx (0.95 and 1.90 μg mL^{-1}). (B) The glucose calibration curve by the modified GOD method. The calibration curve was constructed at the optimized condition.

for subsequent experiments to ensure rapid and complete reaction.

Method validation. A calibration curve for glucose was constructed under the selected conditions (Fig. 8B). The resulting linear relationship was $I_0/I = (0.72 \pm 0.01)C_{glucose} + (-1.73 \pm 0.10)$, $R^2 = 0.999$, over a glucose concentration range of 5.10–15.35 μM. The LOD and LOQ were calculated to be 3.93 and 4.31 μM, respectively. The method was validated following the AOAC guideline. Repeatability and recovery were assessed by testing glucose at concentrations of 5.10, 7.68, and 15.34 μM, with each level measured in seven replicates. All tested concentrations satisfied the AOAC performance criteria for analytical methods (SI Table S5). These results demonstrate the feasibility of employing N-CAdots as a fluorescence sensor for glucose determination *via* a radical scavenging-based mechanism.

Conclusions

This study elucidates the pH-dependent fluorescence behavior of nitrogen-doped citric acid-based carbon dots (N-CAdots) and reveals their previously unreported role as radical scavengers in peroxide-driven reaction systems under mildly alkaline conditions. Determination of the apparent pK_a values of the synthesis system provides mechanism insight into the on–off fluorescence switching of N-CAdots, highlighting the contributions of acidic surface functionalities and the nitrogen-doping. We demonstrate that N-CAdots undergo efficient FL quenching in a mildly H_2O_2–HCO_3^-–Co^{2+} system, in which peroxymonocarbonate (PMC) acts as a key reactive intermediate leading to radical formation. This secondary ROS pathway contrasts with conventional Fenton-type chemistry by offering greater compatibility with biological matrices. Exploiting this mechanism, N-CAdots enable sensitive fluorescence-based detection of H_2O_2 in serum following appropriate optimization. Furthermore, integration with glucose oxidase allows indirect glucose determination *via* enzymatically generated H_2O_2. These fluorescence sensing approaches, based on simple procedures, eliminate the additional carbon footprint associated with the analytical process. Overall, this work establishes N-CAdots as multifunctional nanomaterials that integrate pH-response photophysics with radical-scavenging activity. Beyond analytical sensing, the mechanism insights presented herein may inform the rational design of carbon-dot-based probes and antioxidant systems for broader applications involving controlled reactive oxygen species chemistry.

Conflicts of interest

The authors declare no conflict of interest.

Data availability

All data supporting this study are included in the article and its supplementary information (SI). Supplementary information is available. See DOI: https://doi.org/10.1039/d6ra00349d.

References

1 M. Alafeef, I. Srivastava, T. Aditya and D. Pan, *Small*, 2024, **20**, 2303937.
2 J. Liu, R. Li and B. Yang, *ACS Cent. Sci.*, 2020, **6**, 2179.
3 Y. Kuang, L. Chen, J. Lu, X. Tian, C. Yang, Y. Li, L. Lu and Y. Nie, *New J. Chem.*, 2018, **42**, 19771.
4 K. Nguyen, I.-A. Baragau, R. Gromicova, A. Nicolaev, S. Thomson, A. Rennie, N. Power, M. Sajjad and S. Kellici, *Sci. Rep.*, 2022, **12**, 13806.
5 T. Zhang, Y. Wen, Z. Pan, Y. Kuwahara, K. Mori, H. Yamashita, Y. Zhao and X. Qian, *Environ. Sci. Technol.*, 2022, **56**, 2617.
6 A. Cayuela, M. Soriano, C. Carrillo-Carrión and M. Valcárcel, *Chem. Commun.*, 2016, **52**, 1311.
7 L. Ai, Y. Yang, B. Wang, J. Chang, Z. Tang, B. Yang and S. Lu, *Sci. Bull.*, 2020, **66**, 839.
8 R. Gaikwad, P. Thangaraj and A. Sen, *Sci. Rep.*, 2021, **11**, 2960.
9 N. Di-Marzo, E. Chisci and R. Giovannoni, *Cells*, 2018, **7**, 156.
10 H. Sies and D. Jones, *Nat. Rev. Mol. Cell Biol.*, 2020, **21**, 363.
11 H. Sies, *Redox Biol.*, 2016, **11**, 613.
12 L. Xing, W. Zhang, L. Fu, J. Lorenzo and Y. Hao, *Food Chem.*, 2022, **385**, 132555.
13 J. Pravda, *Mol. Med.*, 2020, **26**, 41.
14 T. Kakeshpour, B. Metaferia, R. Zare and A. Bax, *Proc. Natl. Acad. Sci. U. S. A.*, 2022, **119**, e2121542119.
15 S. Naik, C. Tredwin and C. Scully, *Oral Oncol.*, 2006, **42**, 668.
16 K. Uematsu, *Anal. Sci.*, 2022, **38**, 457.
17 J. Giaretta, H. Duan, F. Oveissi, S. Farajikhah, F. Dehghani and S. Naficy, *ACS Appl. Mater. Interfaces*, 2022, **14**, 20491.
18 J. Todorov, G. McCarty and L. Sombers, *J. Chem. Educ.*, 2023, **100**, 4853.

19 S. Munusamy, T. Mandlimath, P. Swetha, A. Al-Sehemi, M. Pannipara, S. Koppala, P. Shanmugam, S. Boonyuen, R. Pothu and R. Boddula, *Environ. Res.*, 2023, **231**, 116046.
20 T. Niyitanga, K. Ahmad, A. Chaudhary and H. Kim, *Inorg. Chem. Commun.*, 2023, **156**, 111249.
21 M. Lan, Y. Di, X. Zhu, T.-W. Ng, J. Xia, W. Liu, X. Meng, P. Wang, C.-S. Lee and W. Zhang, *Chem. Commun.*, 2015, **51**, 15574.
22 L. Zhou, J. Geng and B. Liu, *Part. Part. Syst. Charact.*, 2013, **30**, 1086.
23 J. Wei, J. Ren, J. Liu, X. Meng, X. Ren, Z. Chen and F. Tang, *Biosens. Bioelectron.*, 2014, **52**, 304.
24 E. V. Bakhmutova-Albert, H. Yao, D. E Denevan and D. E. Richardson, *Inorg. Chem.*, 2010, **49**, 11287.
25 H.-Y. Chen and Y.-F. Lin, *Inorg. Chem.*, 2025, **64**, 554.
26 T. H. Nguyen, T. H. Pham, H. T. Nguyen, N. Nguyen-Bich, N. D. Vu and T. B. V. Nguyen, *Vietnam J. Chem.*, 2022, **60**, 96.
27 W. Szapoczka, A. Truskewycz, T. Skodvin, B. Holst and P. Thomas, *Sci. Rep.*, 2023, **13**, 10660.
28 M. Prado, T. Nguyen and A. Wanekaya, *Sens. Actuators Rep.*, 2023, **6**, 100165.
29 B. Bui-Thi, N. Tran-The, T. Y. H. Bui, T. B. V. Nguyen, V.-T. Ta and N. Nguyen-Bich, *ChemistrySelect*, 2025, **10**, e03165.
30 T. T. Vu, N. D. Vu and T. B. V. Nguyen, *ChemChemTech*, 2025, **68**, 119.
31 L. Wojnarovits, T. Toth and E. Takacs, *Sci. Total Environ.*, 2020, **717**, 137219.
32 A. Charles, *J. Chem. Educ.*, 2023, **100**, 2418.
33 AOAC, *Guidelines for Standard Method Performance Requirements AOAC Official Methods of Analysis, Appendix F*, 2016, vol. 1.
34 C. Wang, T. Hu, Z. Wen, J. Zhou, X. Wang, Q. Wu and C. Wang, *J. Colloid Interface Sci.*, 2018, **521**, 33.
35 Y. Zhang, P. Cui, F. Zhang, X. Feng, Y. Wang, Y. Yang and X. Liu, *Talanta*, 2016, **152**, 288.
36 C. Reckmeier, J. Schneider, Y. Xiong, J. Hausler, P. Kasak, W. Schnick and A. Rogach, *Chem. Mater.*, 2017, **29**, 10352.
37 A. Jonh, *Lange's Handbook of Chemistry*, McGraw-Hill, 15th edn, 1999.
38 M. Raineri, E. Winkler, T. E. Torres, M. V. Mansilla, M. S. Nadal, R. D. Zysler and E. Lima, *Nanosacle*, 2019, **11**, 18393.
39 L. Dul'neva and A. Moskvin, *Russ. J. Gen. Chem.*, 2005, **75**, 1125.
40 C. Shi, C. Li, Y. Wang, J. Guo, S. Barry, Y. Zhang and N. Marmier, *Water*, 2022, **14**, 2309.
41 C. Salvitti, F. Pepi, A. Troiani, M. Rosi and G. Petris, *Molecules*, 2023, **28**, 132.
42 J. Zhang, R. Mani and M. Louhi-Kultanen, *Hydrometallurgy*, 2024, **224**, 106232.
43 S. Patra, A. Mizrahi and D. Meyertein, *Acc. Chem. Res.*, 2020, **53**, 2189.
44 X. Yang, Y. Duan, J. Wang, H. Wang, H. Liu and D. Sedlak, *Environ. Sci. Technol. Lett.*, 2019, **6**, 781.
45 L. Zhou, W. Song, Z. Chen and G. Yin, *Environ. Sci. Technol.*, 2013, **47**, 3833.
46 Y. Zhou, Z. Zhang, Y. Jiang, Z. Shen, P. Zhao and X. Meng, *Appl. Catal., B*, 2025, **362**, 124748.
47 A. Xu, X. Li, S. Ye, G. Yin and Q. Zeng, *Appl. Catal., B*, 2011, **102**, 37.
48 P. Neta, R. Huie and A. Ross, *J. Phys. Chem. Ref. Data*, 1988, **17**, 1027.
49 S. Chen, M. Z. Hoffman and G. Parsons, *J. Phys. Chem.*, 1975, **79**(18), 1911.
50 M. Soriani, D. Pietraforte and M. Minetti, *Arch. Biochem. Biophys.*, 1994, **312**, 180.
51 A. Baschieri, Z. Jin and R. Amorati, *Free Radical Res.*, 2023, **57**, 115.
52 I. Opeida and R. Sheparovych, *Theor. Exp. Chem.*, 2019, **55**, 34.
53 D. Sacks, *Tietz Textbook of Clinical Chemistry and Molecular Diagnostics*, Elsevier, 6th edn, 2017.
54 S. Tummala, R. Bandi and Y.-P. Ho, *Microchim. Acta*, 2022, **189**, 284.
55 F. Honarasa, F. Kamshoori, S. Fathi and Z. Motamedifar, *Microchim. Acta*, 2019, **186**, 234.
56 P. Li, X.-Y. Sun and J.-S. Shen, *Front. Chem.*, 2021, **9**, 713104.
57 Y. Li, X. Gu, J. Zhao and F. Xi, *Molecules*, 2022, **27**, 7379.
58 D. He, C. Zheng, Q. Wang, C. He, Y. Lee, L. Wu and X. Hou, *Talanta*, 2015, **142**, 51.
59 J. Wei, L. Qiang, J. Ren, X. Ren, F. Tang and X. Meng, *Anal. Methods*, 2013, **6**, 1922.